Check for updates

Interactions of limonene and carvone on titanium dioxide surfaces†

Hanyu Fan,‡[a] Elianna S. Frank, [ID] ‡[b] Douglas J. Tobias [ID] *[b] and
Vicki H. Grassian [ID] *[a]

Limonene, a monoterpene, found in cleaning products and air fresheners can interact with a variety of surfaces in indoor environments. An oxidation product of limonene, carvone, has been reported to cause contact allergens. In this study, we have investigated the interactions of limonene and carvone with TiO_2, a component of paint and self-cleaning surfaces, at 297 ± 1 K with FTIR spectroscopy and force field-based molecular dynamics and *ab initio* simulations. The IR absorption spectra and computational methods show that limonene forms π-hydrogen bonds with the surface O−H groups on the TiO_2 surface and that carvone adsorbs on the TiO_2 surface through a variety of molecular interactions including through carbonyl oxygen atoms with Ti^{4+} surface atoms, O−H hydrogen bonding (carbonyl O···HO) and π-hydrogen bonds with surface O−H groups. Furthermore, we investigated the effects of relative humidity (RH) on the adsorption of limonene and carvone on the TiO_2 surface. The spectroscopic results show that the adsorbed limonene can be completely displaced by water at a relative humidity of *ca.* 50% RH ($\sim$2 MLs of water) and that 25% of carvone is displaced at *ca.* 67% RH, which agrees with the calculated free energies of adsorption which show carvone more strongly adsorbs on the surface relative to limonene and thus would be harder to displace from the surface. Overall, this study shows how a monoterpene and its oxidation product interact with TiO_2 and the impact of relative humidity on these interactions.

Introduction

Improving indoor air quality (IAQ) has gained increasing public awareness as people spend most of their time (>90%) indoors compared to outdoors. During the COVID-19 pandemic this was notable, and many people spent more time at home.[1,2] Indoor air pollutants, such as volatile organic compounds (VOCs, *e.g.*, alkanes, alkenes, aromatics, carboxylic acids, alcohols and esters), oxides of nitrogen and sulfur (NO_x and SO_2), carbon monoxide (CO), and particulate matter (PM), including

[a] *Department of Chemistry and Biochemistry, University of California San Diego, La Jolla, California 92093, USA. E-mail: vhgrassian@ucsd.edu*
[b] *Department of Chemistry, University of California, Irvine, California 92697, USA. E-mail: dtobias@uci.edu*

† Electronic supplementary information (ESI) available: The ESI contains 7 figures and 2 tables including: Fig. S1. FTIR spectra of gas-phase limonene; Fig. S2. FTIR spectra of gas-phase carvone; Fig. S3. FTIR spectra of limonene on SiO_2 surface; Fig. S4 and S5. FTIR spectra of limonene and carvone under different RH conditions; Fig. S6. FTIR spectra of water on TiO_2 surface under different pressures; Fig. S7. Density profiles for limonene on each surface; Fig. S8. Snapshots of Hydrogen Bonding Interactions; Fig. S9. Discussion of non-hydroxylated 0.5 ML kink in PMF; Tables S1 and S2. List of simulations for all classical molecular dynamics and all *ab initio* molecular dynamics. See DOI: https://doi.org/10.1039/d2cp03021g

‡ Hanyu Fan and Elianna S. Frank contributed equally to this work.

bacteria and viruses, come from a variety of sources. These sources include consumer products, building materials and furnishings, occupant-related activities (*e.g.*, cleaning, cooking, smoking, breathing), exchange with outdoor air and exhaled breath.[3–6] Secondary products generated from chemical reactions occurring in the gas phase, on particles and on indoor surfaces also contribute to the overall indoor environment.[7,8] Many of these pollutant species and their secondary products can cause allergic reactions, asthma, respiratory diseases, heart disease and lung cancer.[9,10] To improve indoor air quality, besides source control and increasing ventilation, another option is air cleaning.[11,12] Current air treatment techniques include active carbon or zeolite adsorption, biofiltration, ozonation, and advanced oxidation process (AOP) such as non-thermal plasma and photocatalytic oxidation (PCO).[13–15] Among these techniques, PCO is regarded as a potential cost-effective method because its superior features of operation at room temperature and atmospheric pressure to mineralize ppb level of many hazardous gaseous organics to CO_2 and H_2O from indoor air under solar light irradiation without chemical additives required.[16] However, it is important to note that there are unexpected consequences of using these air cleaning processes.[17] Thus, there needs to be testing of these under realistic conditions to further our understanding of the impact on any air cleaning processes.

Titanium dioxide (TiO$_2$) is by far the most widely available semiconductor material used in PCO to its nature abundance, low cost, high chemical stability and safety, and high photo-catalytic activity.[18,19] Rutile and anatase are the two main crystalline structures of TiO$_2$; rutile is the most stable TiO$_2$ phase whereas anatase is more photoactive.[20,21] TiO$_2$-based self-cleaning materials, such as paint films, coated glasses, and tiles, are used both in indoors and outdoors on walls, floors, rooftops and facades.[22] In the state of California, self-cleaning ceramic TiO$_2$ titles are widely used in public places such as hospitals and restrooms.[23] The adsorption and desorption of air pollutants on the surface of TiO$_2$ films are key steps in these heterogeneous photocatalytic oxidation tech-niques. Adsorption is an initial and critical step in the efficient catalytic treatment of all pollutants. In addition, desorption is an essential step to restore the active surface catalytic sites.[24,25] Therefore, to study interaction mechanisms of various VOCs with TiO$_2$ surfaces under relevant indoor environment condi-tions such as the impact of relative humidity is essential to help enhance the photocatalyst performance and understand air pollutants chemistry on indoor surfaces at the molecular level.[26–28]

There are two general modes for VOC adsorption on a TiO$_2$ surface: a weaker physisorption bonding mode with surface Ti–OH groups and a stronger chemisorption bonding mode on Ti^{4+} atoms (Lewis acid sites) or reduced Ti^{3+} sites near oxygen vacancies.[29,30] For example, earlier studies have shown that benzene, toluene, and chlorobenzene can be adsorbed on the TiO$_2$ (rutile) surface via Ti–OH$\cdots\pi$-electron interaction and additional Ti–OH$\cdots$Cl hydrogen bonds for chlorobenzene on the hydroxylated surface and all the above compounds can have Ti$^{4+}\cdots\pi$-electron interaction on the non-hydroxylated surface.[31] The IR absorption spectrum of acetaldehyde onto TiO$_2$ (P25) at 233 K reported that hydrogen bonding with surface OH groups (CH$_3$CH=O$\cdots$HO–Ti) and carbonyl bonding with a Ti^{4+} surface atom (CH$_3$CH=O$\cdots$Ti^{4+}) are the dominant surface interactions.[32] Pyruvic acid adsorbs onto the TiO$_2$ (rutile) sur-face by the interaction between the carboxylic acid group with the surface hydroxyl groups.[33] Similar results were proposed in the study of the TiO$_2$ (P25) surface chemistry with alcohols, organic acids and aldehydes that can be adsorbed onto TiO$_2$ surface via hydrogen bonding to the surface OH groups.[34] The degree of interaction strength between the VOCs and TiO$_2$ surface depends on the relative bonding energies of the hydro-gen bond and is expected to be stronger than π-hydrogen bond. This implies that polar VOCs are more strongly adsorbed onto TiO$_2$ surface.[35–38] For example, the adsorption of different classes of VOCs on TiO$_2$ (P25) surface follows the order of the strength of the corresponding intermolecular forces: *i*-octane < toluene < acetone < methyl ethyl ketone < isopropanol < methanol.[36] Additional insights from the studies of C$_5$–C$_7$ alkanes interactions with TiO$_2$ (P25) surface demonstrated that the larger long-chain and more branched molecules have stronger interactions with the TiO$_2$ surface based on the order of the strength of adsorption: pentane < hexane < *i*-pentane < *i*-hexane < heptane.[39] In another study, the importance of

steric hindrance of different compounds played a role in the interaction strength; it was shown that the adsorption of aromatic species on the TiO$_2$ (P25) surface via following sequence: ethylbenzene < benzene < *o*-xylene < *p*-xylene < *m*-xylene < toluene, while ethyl substitution showed a larger steric hindrance compared to the methyl functional group, so that ethylbenzene is more weakly adsorbed on the TiO$_2$ surface.[40]

Another factor in these studies is the effect of relative humidity. Relative humidity is known to be an important factor in the surface chemistry of environmental interfaces, *i.e.*, interfaces under ambient conditions.[41] There is competition between water vapor and VOCs as well as synergisms.[42–45] For example, there is a respective decrease of 50% and 30% for the adsorption of toluene (80 ppb) and 2-propanol (250 ppb) on TiO$_2$ (anatase) surface at 60% RH compared to the dry condi-tions due to the direct replacement of water adsorption.[42] Other studies reported that the adsorptions of chlorobenzene and cyclohexane on TiO$_2$ (P25) surface significantly decrease with increasing relative humidity, which explains the competition from the water adsorption and further hindrance from the adsorbed water layers.[43,44]

Atomistic simulations provide detailed insight into surface interactions, and in our previous work, we have presented studies of hydroxylated SiO$_2$ (a model for glass surfaces) and indoor relevant organic compounds with great agreement between theory and experiment.[45–47] However, TiO$_2$ presents a unique challenge as there is still outstanding debate over how to model the interactions of water on the TiO$_2$ surface in a simulation, to either represent the water via a molecular or dissociative association on the surface.[48–53] In this study, we have constructed both a non-hydroxylated TiO$_2$ surface with surface Ti atoms and free water molecules, and a fully hydro-xylated TiO$_2$ with all surface Ti atoms capped with OH groups. We use these two surfaces to represent the *extrema* of a real world TiO$_2$ surface. As we find robust agreement between our computational results and the experimental measurements, we are motivated to use our atomistic simulations to suggest relevant surface interactions between TiO$_2$ and organic mole-cules, however these insights only serve to deepen the conclu-sions made from the experimental results.

Among the many VOCs present indoors, limonene is widely used in cleaning products and air fresheners to provide a pleasant smell. Our previous studies showed that limonene forms one or two Si–OH$\cdots\pi$-hydrogen bonds on the hydroxy-lated SiO$_2$ surface, and more than 50% of limonene remains adsorbed within the water and hydroxylated SiO$_2$ surface through H–OH or Si–OH$\cdots\pi$-hydrogen bonding at a relatively high 78% RH when the water coverage is close to three mono-layers (MLs); carvone forms a Si–OH$\cdots$O hydrogen binding and an oxygen silicon association with siloxane bridge (O$\cdots$Si–O–Si) on the hydroxylated SiO$_2$ surface, and instead of replacing the adsorbed carvone on SiO$_2$ surface, water adsorbs onto the carvone coverage via H–OH$\cdots$O hydrogen binding.[45–47] To the best of our knowledge, there are no systematic studies with respect to the adsorption of limonene and its oxidation product

This journal is © the Owner Societies 2022

Phys. Chem. Chem. Phys., 2022, **24**, 23870–23883 | **23871**

carvone on TiO$_2$ surface or the impact of relative humidity over a wide range of relative humidity conditions. In the present work, we combined transmission FTIR spectroscopy, classical force field-based and *ab initio* molecular dynamics simulations to investigate the types of surface interactions and relative strengths of limonene and carvone adsorbed on the hydroxylated TiO$_2$ surface. The effect of relative humidity ranging from <1% to 67% RH on the interactions of limonene and carvone on the hydroxylated TiO$_2$ surface was also investigated.

Experimental and theoretical methods

Experimental methods

TiO$_2$ (rutile, high purity, 99.9+%, Stock#: US3520) was purchased from US Research Nanomaterials, Inc. The surface area measurements of TiO$_2$ particles were done using a Quantachrome Nova 4200e multipoint Brunauer–Emmett–Teller (BET) surface analyzer. First the TiO$_2$ particles were degassed overnight at 120 °C prior to a BET measured. The average BET surface area and standard deviation was determined to be 17 ± 1 m^2 g^{-1}. The limonene (D-limonene, >99%, Fisher Scientific) and carvone (D-carvone, >98%, TCI) samples were prepared by degassing three times with consecutive freeze–pump–thaw cycles.

The experimental infrared setup has been described previously.[45–47] Approximately 8 mg of TiO$_2$ was pressed onto to a tungsten grid with a stainless-steel press. The TiO$_2$ particles were calcined at 200 °C in an oven for 2 hours prior to pressing onto the grid. The grid with particles was held in position by nickel jaws inside of the stainless-steel IR cell with BaF$_2$ windows. The rest of the experimental setup consists of a stainless IR cell (310 ± 3 ml, the optical path length of the IR cell is 7 cm), a glass mixing chamber (1329 ± 2 ml), a stainless-steel connection tubing (length: 36 inch and I.D. 1/4 inch) and a two-stage vacuum system (a turbomolecular pump (Agilent TwisTorr 74 FS) with a backup mechanical pump (Adixen Pascal 2010 SD)). Two absolute pressure transducers (MKS Instruments, Inc., 10 and 1000 Torr) were used to record the equilibrium pressure data.

FTIR spectra were recorded with a Nicolet iS50 FTIR spectrometer (Thermo Fisher Scientific). Prior to and under the equilibrium exposure of organic compound vapor, single-beam spectra (300 scans) of the respective particles surface and gas phase were acquired using at a spectral resolution of 4 cm^{-1} over the spectral range of 1200–4000 cm^{-1}. The surface absorbance spectra were obtained by subtracting the FTIR spectra of gas-phase organic compound from the particles surface plus gas-phase spectra. To investigate the effects of RH, the particles sample was first exposed to the organic vapor for 50 min under dry condition (<1% RH); followed by the introduction of water vapor into the IR cell for 1 minute; and then the IR cell was closed for another 50 minutes for the equilibrium before the particles surface were evacuated for the desorption measurement. The % RH values were recorded based on the water vapor pressure reading after 1 minute water

injection. The water vapor reached equilibrium in the IR cell within 1 minute once the water vapor was injected.[45]

Computational methods

Force field-based MD simulations and *ab initio* MD (AIMD) simulations were used to investigate the adsorption of limonene and carvone on a TiO$_2$ surfaces. For both simulation methods, a 110 rutile TiO$_2$ unit cell was replicated in the *x*, *y* and *z* directions to create the initial structure.[54] Due to the outstanding debate over the nature of the interactions of water on the TiO$_2$ surface, force field-based MD simulations for both a non-hydroxylated TiO$_2$ surface with surface Ti atoms and free TIP3P water molecules and a fully hydroxylated TiO$_2$ with no surface Ti atoms have been prepared.[48–52] For our AIMD simulations, we have prepared three surfaces, a non-hydroxylated TiO$_2$ surface, a TiO$_2$ surface with 4 water molecules between the adsorbate and the surface, and a fully hydroxylated TiO$_2$ surface. However, because these AIMD simulations were all run at 300 K, some of the O–H groups on the fully hydroxylated surface underwent dissociations during the course of the AIMD simulation.

For the force field-based MD simulations, a 35 × 40 × 21 Å^3 TiO$_2$ slab was created and 77 Å of vacuum was placed separating the upper and lower surfaces in the *z* direction. From this initial surface with 720 Ti atoms and 1440 O atoms, the non-hydroxylated and hydroxylated TiO$_2$ surfaces were produced. For clarity, we can consider all TiO$_2$ surfaces consisting of two parts, the frozen core Ti and O atoms and the surface atoms. In the case of the non-hydroxylated surface, the surface atoms are the bridging oxygen atoms and 5-coordinated Ti atoms. In the case of the hydroxylated surface, all atoms on the top and bottom of the surface were hydroxylated, thus the surface atoms are the surface OH groups. To investigate the role of %RH, TIP3P water was added to both sides of the TiO$_2$ surface, which in the text we will refer to as the 0.5 monolayer and 1 monolayer systems. The 0.5 monolayer system was represented by a total of 204 water molecules, corresponding to number of bridging oxygen atoms in the non-hydroxylated surface. The 1 monolayer system was represented by 408 water molecules.

The force field produced by Brandt *et al.* was used for the non-hydroxylated surface.[55] For the hydroxylated surface, the nonbonded parameters were set to 0 for hydrogen and in order to ensure a neutral surface, the partial charge of all hydrogen atoms was set to +0.44175*e*. And the O–H group oxygen partial charge was set to −0.80*e*. During the course of the simulation, all bulk atoms were frozen, and all surface atoms were allowed to move freely. There were small distortions of the TiO$_2$ surface as seen in the molecular snapshots in Fig. 3, however the general structure of the TiO$_2$ crystal was retained. The TIP3P water was used to describe the water molecules and details of the CHARMMM compatible force fields for limonene and carvone can be found in our previous work.[46,47,56]

All classical molecular dynamics simulations were done with the LAMMPS[57] software package. The equations of motion were integrated using the velocity Verlet algorithm with a

23872 | *Phys. Chem. Chem. Phys.*, 2022, **24**, 23870–23883

This journal is © the Owner Societies 2022

1 fs time step.[58] Electrostatic interactions were evaluated directly up to a cutoff of 12 Å and with a particle–particle–particle mesh solver with a relative accuracy of 10^{-6}.[59] Lennard-Jones interactions were cut off after 12 Å. The simulation temperature was maintained at 300 K using a Nosé–Hoover thermostat with a relaxation time of 100 fs.[60]

Umbrella sampling was used to calculate the free energy profile for the desorption of carvone and limonene from the TiO$_2$ surfaces.[61] Initial coordinates of each adsorbate on the TiO$_2$ surface were taken after 25 ns of simulation time. The distance of the center-of-mass of adsorbate to the TiO$_2$ surface was used as the reaction coordinate, and the process was divided into variable number of windows for each adsorbate. For limonene, 22 windows in 0.50 Å increments was sufficient, but for carvone, 0.25 Å increment windows were used. A harmonic restraining potential of 10 kcal mol^{-1} Å^{-2} was applied in each window. Each free energy profile was generated from 30 ns or longer long biased trajectories for each PMF window using the WHAM scheme.[62]

In the hydroxylated surface, two forms of hydrogen bonding were considered, π-hydrogen bonds formed between carbon sp^2 (C$_{sp^2}$) atoms and the TiO$_2$–OH surface for both limonene and carvone, and hydrogen bonds formed between the carvone oxygen atoms and the TiO$_2$–OH surface. To calculate these hydrogen bonding probabilities, distances were measured between C$_{sp^2}$ centers and surrounding oxygen donors and between the carvone oxygen atom and surrounding oxygen donors. Angular measurements were made between adsorbate acceptor (C$_{sp^2}$ center or carvone oxygen atom), TiO$_2$ donor H, and TiO$_2$ donor O atoms. All measurements were made every 1 ps. Hydrogen bonds were defined to be present if the distance between donor and acceptor was less than 3.5 Å and if the angle between acceptor, donor H, and donor O was within 120–180 degrees for both types of hydrogen bonds. Additionally, in systems with free water molecules, π-hydrogen bonds between C$_{sp^2}$ centers and water molecules, as well as hydrogen bonds between the carvone oxygen atom and water were measured in the same way as described above.

For the *ab initio* simulations, three TiO$_2$ surfaces were studied, a non-hydroxylated surface, a hydroxylated surface, and a non-hydroxylated surface with 4 water molecules placed between the surface and the adsorbate. The TiO$_2$ surface was obtained from selecting a smaller portion of the classical MD surface. For all simulations expect for carvone on the non-hydroxylated surface with 4 water molecules, a system of 90 Ti atoms and 180 O atoms, accounting to 5 layers of Ti and O atoms, was sufficient to allow for ample simulation time (30 ps). In the case of carvone on the non-hydroxylated surface with 4 water molecules, a slightly larger size in the y direction of the TiO$_2$ surface (125 Ti atoms and 250 O atoms) was used. This resulted in eight AIMD simulations, detailed in the ESI.† In the case of the hydroxylated surface and the non-hydroxylated surface with water molecules, only the top of the surface was either hydroxylated or had water molecules placed on top, to save computational time.

For all systems, a 30 ps AIMD simulation at 300 K with a time step of 0.5 fs was performed, except for the carvone on the non-hydroxylated surface with 4 water molecules, where at 13 ps AIMD simulation at 300 K with a time step of 0.5 fs was performed. The temperature as maintained at 300 K using a Nose–Hoover[14] thermostat with a relaxation time of 100 fs. The PBE[63] exchange–correlation functional with the DZVP-MOLOPT-SR-GTH[64,65] basis set and the GTH pseudopotentials in the QUICKSTEP module of the CP2K[66] package were used. A SCF convergence criterion of 10^{-6} (a.u.) with the orbital transformation[67] scheme and DIIS minimization[68] were used in each simulation. All systems were placed in orthorhombic boxes under periodic boundary conditions in the x and y directions with the z direction normal to the TiO$_2$ surface. The AIMD simulation cells had sizes of 15.960 Å × 12.638 Å × 36.821 Å and for the slightly larger system for carvone on the non-hydroxylated surface with 4 water molecules, the cell size was 15.091 Å × 16.437 Å × 36.821 Å. During the course of the simulation, the bottom half of the TiO$_2$ surface was frozen.

The power spectra were calculated for the Fourier transform of the velocity autocorrelation function of all oxygen or hydrogen atoms using the TRAVIS code.[69,70] A 900 fs Gaussian windowing function was applied to the correlation function prior to Fourier transformation.

Results and discussion

Experimental data

Surface adsorption of limonene under dry conditions ($<1\%$ RH). Fig. 1(a) shows FTIR absorbance spectra of limonene adsorbed on TiO$_2$ as a function of varying pressure (3, 6, 11, 20, 31, 42, 75 and 148 mTorr) at 297 ± 1 K under dry conditions ($<1\%$ RH). For these spectra, the clean TiO$_2$ surface prior to adsorption was used as the background spectrum and, in addition, gas-phase contributions were subtracted from each of the spectra. The observed IR absorption band frequencies are close to that found for gas-phase limonene (see Fig. S1, ESI†). The absorption bands at 3085, 3074, 3010 cm^{-1} are due to the C–H stretching motions for olefinic C–H modes. The absorption bands at 2968, 2922, 2860, and 2838 cm^{-1} are due to the aliphatic C–H stretching modes. The 1644 cm^{-1} band is assigned to the C=C stretching vibration of the vinyl group and in the ring. The absorptions observed at 1454, 1439, and 1378 cm^{-1} for CH$_3$ and CH$_2$ bending vibrations motion, respectively.[45,46] In addition, the negative peak at 3656 cm^{-1} is attributed to the loss of Ti–OH groups due to the hydrogen-bonding interactions with limonene, as a broad peak centered at $\sim$3447 cm^{-1} grows in with increasing limonene pressure.

Fig. 1(b) displays the integrated absorbance of the C–H stretching region (ranging from 2800 to 3115 cm^{-1}) and the loss of Ti–OH function groups peak height (3656 cm^{-1}, right ordinate) as function of limonene pressure. It is observed that no apparent increases in the amount of the adsorbed limonene after 60 mTorr as there are no more free Ti–OH functional groups present on the TiO$_2$ surface. This finding indicates that the adsorption of limonene on the hydroxylated TiO$_2$ surface is mainly *via* the Ti–OH$\cdots$π-electron interaction. Our earlier study

This journal is © the Owner Societies 2022

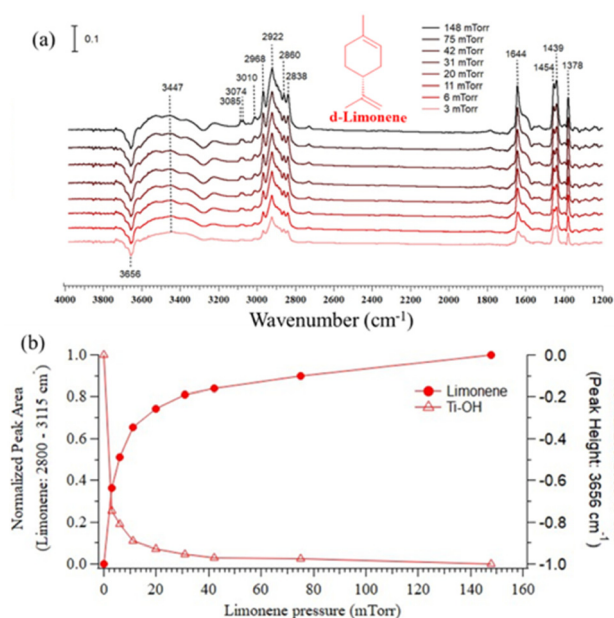Phys. Chem. Chem. Phys., 2022, **24**, 23870–23883 | **23873**

Fig. 1 (a) FTIR spectra of limonene adsorbed on TiO$_2$ surface under dry conditions (<1% RH) as a function of limonene pressure in the spectral range extending from 1200 to 4000 cm^{-1} (scale bar = 0.1 absorbance units). The equilibrium pressures increase from the light red to black spectra: 3, 6, 11, 20, 31, 42, 75, and 148 mTorr. (b) The ordinate plots the normalized integrated peak area of limonene in the spectral region from 2800 to 3115 cm^{-1} as function of limonene pressure (mTorr), the right ordinate plots the normalized peak height of the loss of Ti–OH functional groups at 3656 cm^{-1}.

shows that the interactions between limonene and hydroxylated SiO$_2$ surface are mainly driven by Si–OH$\cdots\pi$-hydrogen bonding.[45] The desorption free energies of limonene from TiO$_2$ and SiO$_2$ surface are discussed in the computational results section below.

Surface adsorption of carvone under dry conditions (<1% RH). Fig. 2(a) shows the IR absorbance spectra of carvone on the TiO$_2$ surface at equilibrium pressures of 2, 8 and 18 mTorr under dry conditions (<1% RH), using the TiO$_2$ surface as the background and with gas-phase contributions subtracted from the spectra. The IR spectra shows that carvone adsorbs to the TiO$_2$ surface *via* hydrogen bonding as shown by the loss of Ti–OH groups at 3656 cm^{-1} and the red-shifted broad peak at 3362 cm^{-1}. The observed IR surface absorption band frequencies are in agreement with the gas-phase carvone vibrational frequencies (see Fig. S2, ESI†) except for the shifts in the spectral range extending from *ca.* 1560 to 1720 cm^{-1}. The absorption bands at 3086, 3074 cm^{-1} and 3021 cm^{-1} are for the C–H sp^2 stretching motion from alkene and ring; the bands at 2968, 2927, 2893, and 2857 cm^{-1} are for the C–H sp^3 stretching motion; the bands at 1453, 1435 and 1378, 1373 cm^{-1} are for CH$_3$ and CH$_2$ bending vibrations motion, respectively; and the big broad band at 1648 cm^{-1} is attribute to the coupling of C=O (ketone) and C=C (alkene) stretching vibrations.[47] As shown in Fig. 2(b), there is a growth of new band at 1683 cm^{-1} starting at 8 mTorr. This higher energy shift of 35 cm^{-1} can be explained by considering the interaction of
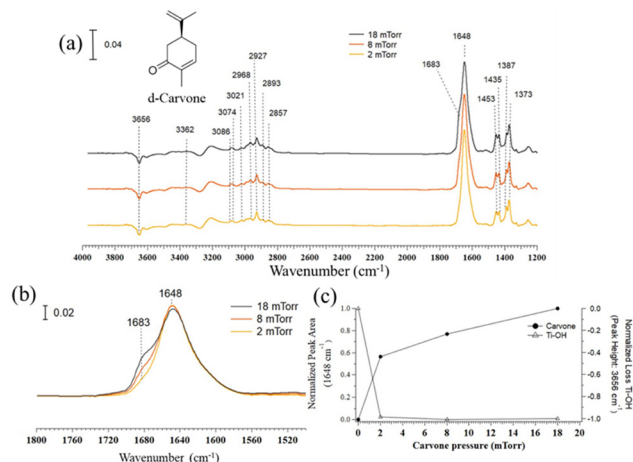

Fig. 2 (a) Absorbance FTIR spectra of carvone adsorbed on TiO$_2$ surface under dry conditions (<1% RH) as a function of pressure in the spectral range extending from *ca.* 1200 to 4000 cm^{-1} (scale bar = 0.04 absorbance units). (b) The above (a) spectra range extends from 1500 to 1800 cm^{-1} (scale bar = 0.02 absorbance units). (c) The ordinate plots the normalized integrated peak area of carvone at 1648 cm^{-1} (ranging from 1560 to 1720 cm^{-1}) as function of carvone pressure (mTorr), the right ordinate plots the normalized peak height of the loss of Ti–OH function groups at 3656 cm^{-1}. The equilibrium pressures are 2, 8, and 18 mTorr, respectively.

adsorbed carvone molecules can be through carbonyl bonding with a Ti^{4+} surface atom on the TiO$_2$ surface.[32,47] Fig. 2(c) displays the integrated peak area of adsorbed carvone at 1648 cm^{-1} (ranging from 1560 to 1720 cm^{-1}) and the loss of Ti–OH functional groups peak height at 3656 cm^{-1} (right ordinate) as function of different equilibrium carvone pressures. It is observed that almost all the free Ti–OH functional groups are occupied by carvone molecules at a low equilibrium pressure of 2 mTorr. As the carvone pressure is changing from 8 mTorr to 18 mTorr with an increase of 10 mTorr, there is about 30% of amount carvone increased on TiO$_2$ surface. In Fig. 1(b), when the limonene pressure is changing from 75 mTorr to 148 mTorr with an increase of 73 mTorr, there is only 10% of amount limonene is increased on TiO$_2$ surface. Once monolayer coverage on the TiO$_2$ surface is reached, the $\frac{\Delta \text{ increase amount of adsorbate}}{\Delta \text{ increase pressure}}$ (% mTorr^{-1}) ratios of carvone and limonene are 3 and 0.14, respectively. This observation suggests that the adsorption of carvone on the TiO$_2$ surface is initially *via* the O–H hydrogen bonding (carbonyl O$\cdots$HO–Ti) and the Ti–OH$\cdots\pi$-electron interaction; and once all the available Ti–OH groups are occupied in hydrogen bonds, the later adsorption of carvone on TiO$_2$ surface is through a strong carbonyl bonding with a Ti^{4+} surface atom.[47] Although these binding interactions are different, in the discussion above we make the assumption that the increase in intensity is linearly proportional to coverage.

Limonene and carvone adsorption on TiO$_2$ at higher relative humidity (>1% RH). The impact of relative humidity was further explored for limonene and carvone adsorption on TiO$_2$. In these experiments, the TiO$_2$ surface was first exposed to either limonene or carvone and then following this water

23874 | *Phys. Chem. Chem. Phys.*, 2022, **24**, 23870–23883

This journal is © the Owner Societies 2022

Table 1 Changes in adsorbed limonene and carvone on TiO$_2$ surface as a function of relative humidity and co-adsorbed water

Percent relative humidity ($\pm 1\%$)	Water coverage in monolayers (MLs) (± 0.1)[a] (bare TiO$_2$ surface)	Percentage of organic compound remaining on surface relative to dry conditions ($\pm 3\%$)[bc]	Water coverage in monolayers (MLs) (± 0.1) (with organic compound adsorbed on TiO$_2$ surface)[d]
Limonene			
<1	<0.1	100	<0.1
3	0.5	91	0.3
10	1.0	74	0.5
18	1.4	67	0.8
25	1.6	54	1.6
30	1.7	30	1.7
51	2.0	0	2.0
Carvone			
<1	<0.1	100	<0.1
67	2.3	75	0.6

[a] Water coverages determined from Goodman et al.[71] [b] Percent limonene coverages determined from the integrated absorbance of bands from 1415 to 1475 cm^{-1}. [c] Determined from the integrated absorbance ranging from 1335 to 1490 cm^{-1} for carvone. [d] Water coverages estimated from relative ratio of the integrated area of the water bending mode when the organic compound is present relative to the bare surface.

vapor was introduced into the infrared cell at different relative humidity. In the case where water displaces organic compounds from the surface, there is the growth of adsorbed water absorption bands on the surface concomitant with a loss of adsorbed organic compound from the surface. When water co-adsorbs, there is the growth of adsorbed water absorption bands on the surface with little or no change in the amount of adsorbed organic compound. Finally, if the organic compound blocks water adsorption there will be little change in the spectrum. To quantify which of these different is occurring, we determined the change in coverage of the organic compound – either limonene or carvone – on the surface at different relative humidity compared to under dry conditions. We also determined the amount of water adsorbed on the surface at this different relative humidity (see Fig. S6, ESI†). Table 1 shows these results for both limonene and carvone (see also Fig. S4 and S5 in ESI†). For limonene, it is seen that the coverage decreases significantly with increasing percent relative humidity while the amount of water adsorbed on the surface increases. These data show that water displaces limonene from the surface into the gas phase. For carvone, there is little change in the surface coverage of carvone as a function of relative humidity and, additionally, little water is taken up by the surface. Overall, these data show that carvone, the oxidation product of limonene, is not easily displaced and also more strongly interacts with the surface compared to limonene.

MD simulations data

Surface interactions: classical molecular dynamics (MD) and *ab initio* molecular dynamics (AIMD) results. To elucidate the interactions between each adsorbate and the TiO$_2$ surface from an atomistic perspective, two kinds of MD simulations were performed. Force field-based molecular dynamics simulations were used to calculate the free energy profile for the desorption of each adsorbate on the TiO$_2$ surface, as well as to calculate various surface interactions (hydrogen, π-hydrogen, carbonyl O–Ti interactions). *Ab initio* MD (AIMD) simulations were used to construct the power spectra of carvone and limonene adsorbed on the TiO$_2$ surface and to further investigate the

carvone carbonyl O–Ti interaction. For each MD surface, we constructed a 50 ns unbiased MD simulation, and molecular snapshots shown in Fig. 3 show limonene and carvone on the TiO$_2$ with differing monolayers (ML) of water.

During the course of the 50 ns simulation, we observed the carvone cyclic ring of carvone and limonene predominantly stays parallel to the surface for the non-hydroxylated 0 ML H$_2$O and 0.5 ML H$_2$O surfaces and the hydroxylated 0 ML H$_2$O surface. In the hydroxylated 0.5 ML H$_2$O surface, the limonene ring was able to freely rotate on the surface. In both the non-hydroxylated and hydroxylated 1 ML H$_2$O surfaces, the limonene ring and carvone ring were able to freely rotate above the surface. On the non-hydroxylated 0 ML H$_2$O surface, we observed that both limonene and carvone stayed between two rows of bridging oxygen atoms for the course of the 50 ns simulation.

A second relevant measure of surface interactions are the formation of hydrogen bonds. As discussed in the introduction, we have studied the importance of hydrogen bonds to promote stabilization between indoor relevant organic compounds and indoor surfaces. We have studied the role of two kinds of hydrogen bonds, π-hydrogen bonds formed between C$_{sp^2}$ carbon centers and surface OH groups and hydrogen bonds formed between the carvone oxygen atom and surface OH groups. To investigate the adsorption of limonene and carvone on TiO$_2$ surface, we have calculated the average number of π-hydrogen bonds during the course of the last 25 ns of the unbiased simulations. π-hydrogen bonds require hydrogen atoms as hydrogen bond donors, so no measurements were made for the non-hydroxylated surface with 0 ML H$_2$O, but the results for the rest of the surfaces are displayed in Table 2.

Overall, we see the formation of fewer π-hydrogen bonds with water molecules compared to our similar study of limonene on hydroxylated SiO$_2$ surface with increasing %RH (average of 0.30 for limonene on SiO$_2$ with 1 MLs H$_2$O *versus* 0.17 for limonene on hydroxylated TiO$_2$ with 1 MLs H$_2$O). This is due to the fact that not only are water–water hydrogen bonds more favorable compared to π-hydrogen bonds, but water hydrogen bonds to TiO$_2$ for either the non-hydroxylated or hydroxylated
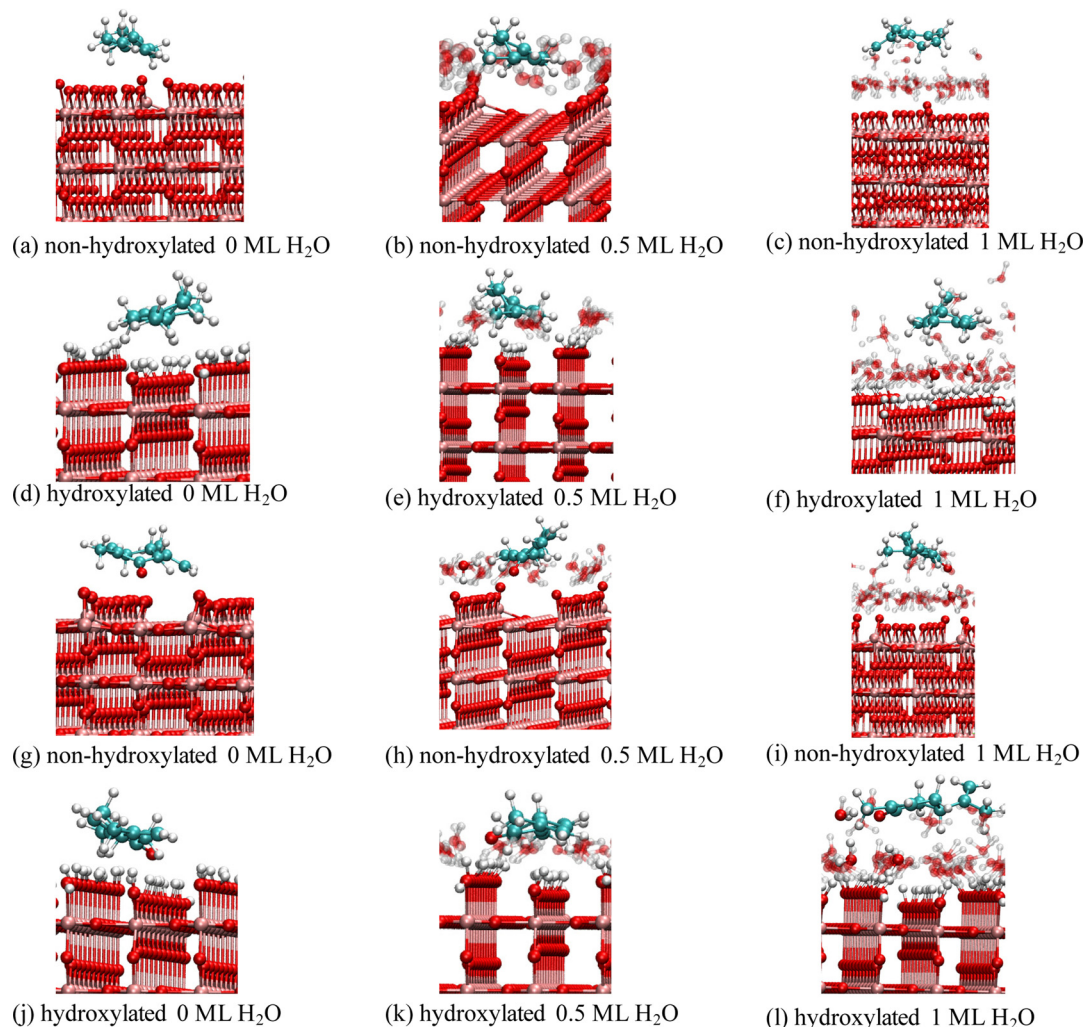
Fig. 3 (a–c) Shows limonene on non-hydroxylated TiO$_2$ surfaces with increasing levels of hydration, (d–f) shows limonene on hydroxylated surfaces with increasing levels of hydration, (g–i) shows carvone on non-hydroxylated TiO$_2$ surfaces with increasing levels of hydration, (j–l) shows carvone on hydroxylated TiO$_2$ surfaces with increasing levels of hydration. Water molecules engaged in hydrogen bonds (π-hydrogen or OH-hydrogen) with the adsorbate are shown in full color, all other water molecules are shown transparent. Red atoms correspond to O atoms, pink atoms correspond to Ti atoms, white atoms correspond to H atoms and cyan atoms correspond to C atoms. The surfaces have been oriented to easiest see surface/adsorbate interactions.

surface are also quite strong, resulting in fewer water donor π-hydrogen bonds to limonene and carvone C$_{sp^2}$ carbon atoms. We see on the hydroxylated surfaces that there are more surface to adsorbate π-hydrogen bonds, and these interactions occur frequently for the 0 ML H$_2$O and 0.5 ML H$_2$O surface. For the 1 ML H$_2$O surface, C$_{sp^2}$ carbon atoms on the adsorbate are too far away in the water layer to interact with the OH groups on the surface.

Limonene and carvone both have two double bond sites and we found that the endocyclic C=C bond always has a higher probability of π-hydrogen bond formation, and this is because the exocyclic C=C bond sometimes rotates above the water layer. Finally, there is a clear difference in π-hydrogen bonding probabilities between these two molecules, as the limonene molecule is much more likely to form π-hydrogen bonds compared to the carvone molecule. This does not indicate that

limonene has a stronger interaction with the surface, but rather that carvone shows a much lower propensity for π-hydrogen bond formation. This is due to stabilizing hydrogen bonds formed between the carvone oxygen atom and TiO$_2$ surface. Table 3 shows the carvone carbonyl oxygen atom hydrogen bonding statistics.

In Table 3, we see few water carvone hydrogen bonds are formed for the non-hydroxylated 0.5 ML H$_2$O surface, which we attribute to the increase in stabilization for water–water and water–surface hydrogen bonds as discussed above. However, we see with 1 ML of water there is an average of around 0.80 hydrogen bonds between carvone and the surrounding water, regardless of the surface hydroxylation. As shown in Table 3, accounting for both π-hydrogen and hydrogen bonds, there are more surface interactions for the carvone molecule compared to those of limonene. This is consistent with our experimental

23876 | *Phys. Chem. Chem. Phys.*, 2022, **24**, 23870–23883

This journal is © the Owner Societies 2022

Table 2 Average number of π-hydrogen bonds for carvone and limonene. π-Hydrogen bonding criteria was determined if the C_{sp^2}–O distance was less than 3.5 Å and the OH···C_{sp^2} angle was >120°. (n. a. – not applicable)

Surface	Water (ML)	Hydrogen bond donor	Average number of π-hydrogen bonds	
			Limonene	Carvone
Non-hydroxylated	0.5	Surface	n. a.	n. a.
		Water	0.0049	0.0085
Non-hydroxylated	1	Surface	n. a.	n. a.
		Water	0.13	0.05
Hydroxylated	0	Surface	0.28	0.15
		Water	n. a.	n. a.
Hydroxylated	0.5	Surface	0.66	0.43
		Water	0.017	0.005
Hydroxylated	1	Surface	0	0
		Water	0.17	0.07

Table 3 Carvone carbonyl oxygen atom hydrogen bonding statistics. Hydrogen bonding criteria was determined if the O–O distance was less than 3.5 Å and the OH···O angle was >120°. (n. a. – not applicable)

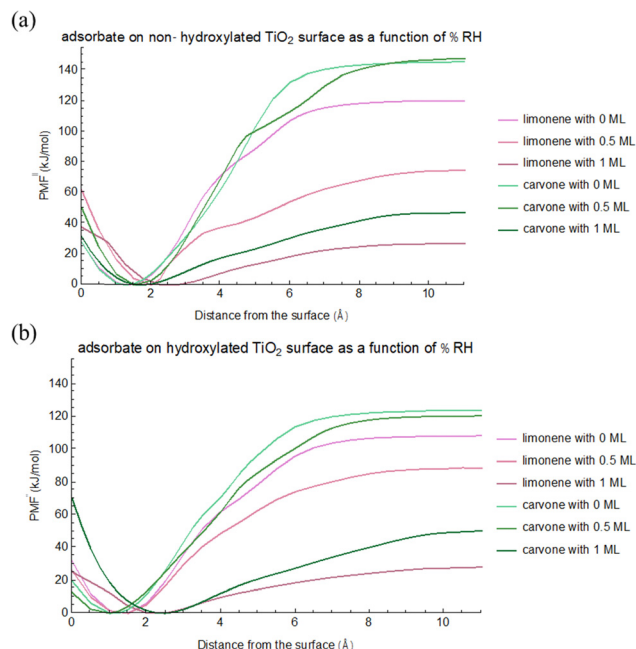| Surface	Water (ML)	Hydrogen bond donor	Average number of Hydrogen bonds
Non-hydroxylated	0.5	Surface	n. a.
		Water	0.08
Non-hydroxylated	1	Surface	n. a.
		Water	0.80
Hydroxylated	0	Surface	1.57
		Water	n. a.
Hydroxylated	0.5	Surface	2.2
		Water	0.18
Hydroxylated	1	Surface	0.0018
		Water	0.76

Fig. 4 (a) Potential of mean force for the desorption of limonene and carvone from non-hydroxylated surface calculated. (b) Potential of mean force for the desorption of limonene and carvone from hydroxylated surface. Both are calculated from the classical molecular dynamics simulations.

results that indicate carvone has stronger interactions with the TiO₂. As we will discuss in detail in the *ab initio* MD simulation results section, there is an additional surface interaction between the carvone carbonyl oxygen atom and the surface Ti atoms in the non-hydroxylated surface. In this case, we have detected that during the course of the 50 ns non-hydroxylated 0 ML H₂O simulation, the carvone carbonyl oxygen is positioned close to surface Ti atoms with an average interaction length of 3.92 Å. More importantly, our *ab initio* power spectra support the validity of this interaction as there is a red shift in the C=O bond length compared to the gas phase carvone spectra. With the presence of water the carvone carbonyl oxygen–Ti surface

interaction rapidly decreases, as with 0.5 ML of water, only 8% of the 50 ns trajectory shows nearest neighbor to the carvone carbonyl oxygen is a surface Ti atom. A key benefit of atomistic MD simulations is the ability to study the arrangement of large numbers of molecules. In this case, we can investigate the hydrogen bonding network between water molecules and the TiO₂ surface, and how this is disrupted by the adsorption of limonene and carvone molecules. As our molecular snapshots show, water is adsorbed on the surface *via* hydrogen bonds to surface O atoms and surface OH groups and water molecules are also stabilized by water–water hydrogen bonds. Table 4 shows the extent that limonene and carvone disrupt the hydrogen bonding network by measuring the interactions of water molecules engaged in hydrogen bonding with the adsorbate. In some instances, the water molecule is able to form a hydrogen bond with the adsorbate and also a hydrogen bond with the surrounding water molecules or surface. In other

Table 4 Fraction of water–water hydrogen bonds, water–surface hydrogen bonds, and water–adsorbate hydrogen bonds. A hydrogen bond is defined as the O–O distance 3.25 Å and angle >120°

| Surface	Water (ML)	Adsorbate	Fraction of bonding waters in water–water bonds	Fraction of bonding waters in water–surface bonds	Fraction of bonding waters only in adsorbate bonds
Non-hydroxylated	0.5	Limonene	0.50	0.47	0.03
		Carvone	0.58	0.39	0.02
Non-hydroxylated	1	Limonene	0.80	0.17	0.03
		Carvone	0.95	0.046	0.003
Hydroxylated	0.5	Limonene	0.32	0.678	0.002
		Carvone	0.511	0.486	0.003
Hydroxylated	1	Limonene	0.66	0.34	—
		Carvone	0.758	0.24	0.002
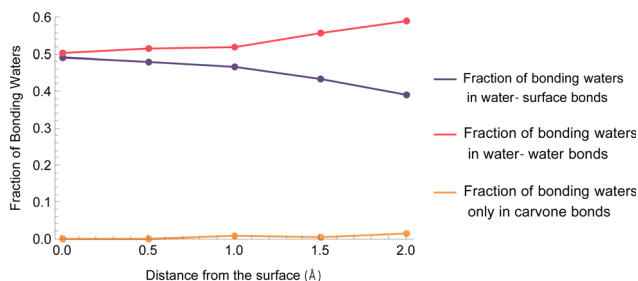
Fig. 5 Fraction of water molecules in hydrogen bond interactions with carvone that are also in hydrogen bonds with either the TiO_2 surface, surrounding waters, or no other molecules (thus disrupting the hydrogen bonding network) as a function of distance from the surface during the PMF calculation.

cases, the hydrogen bonding network is "disrupted" as the water molecule is only engaged in a hydrogen bond with the adsorbate. Snapshots of these hydrogen bonding interactions are shown in Fig. S8 (ESI†). These networks are also seen in our *ab initio* simulations.

Table 4 shows the difference in hydrogen bonding networks for the limonene and carvone molecules. Overall, this table shows that limonene forms more π-hydrogen bonds with water molecules engaged in hydrogen bonding with the TiO_2 surface. Given the competitive adsorption of water on the TiO_2 surface,

this suggests why limonene is displaced at high %RH. Contrary, carvone is shown to more often form hydrogen and π-hydrogen bonds with water molecules also in hydrogen bonding with other water molecules. In addition, in the case of the non-hydroxylated surface, limonene is shown to disrupt the hydrogen bond network more compared to that of carvone. This suggests why there is little change in the surface coverage of carvone as a function of %RH. To further quantify the difference in interaction strength, we have calculated the free energy profile (also referred to as potentials of mean force or PMF) for the desorption of the adsorbate from the surface, as shown in Fig. 4. The free energy profiles are placed vertically, such that their minima are at the zero of free energy.

We first note that these desorption free energies are substantially higher than our previous results for SiO_2. This is to be expected as the partial charges of surface Ti and O atoms are much higher compared to those of SiO_2. However, the trend of greater free energies of desorption compared to SiO_2 are consistent with the experimental measurements of much longer desorption lifetimes for limonene and carvone on the TiO_2 surface. As seen in Fig. 4(a), the desorption free energy for carvone on the non-hydroxylated with 0 ML H_2O is ~ 30 kJ mol^{-1} higher than limonene. This is consistent with our experimental measurements, and our calculations suggest is due to the close interaction between the carvone oxygen and
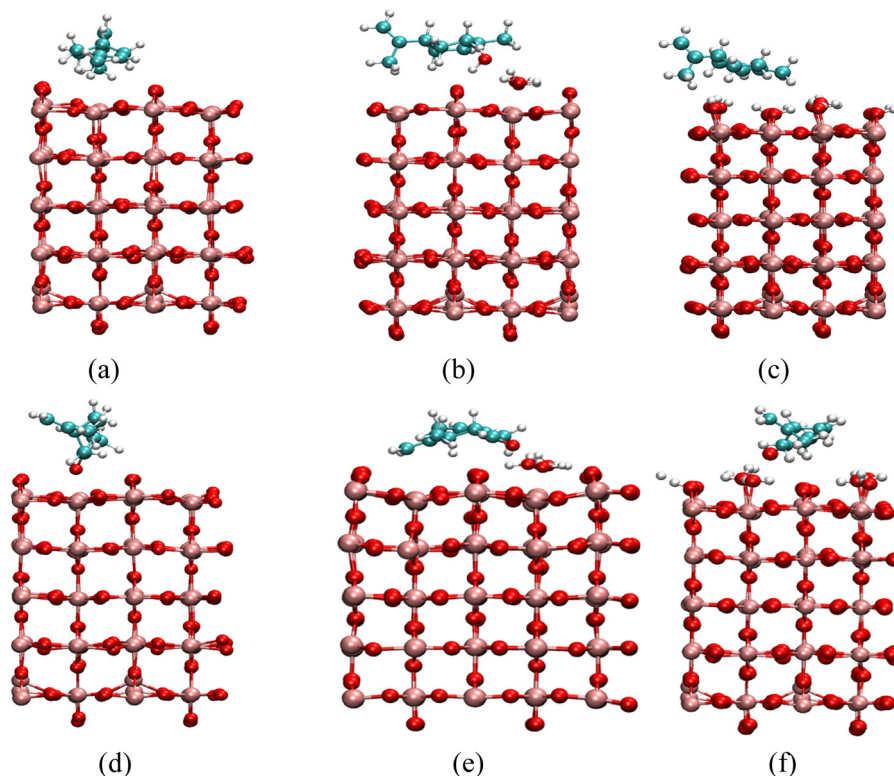

Fig. 6 (a–c) Shows limonene on a non-hydroxylated surface with 0 water molecules, on a non-hydroxylated surface with 4 water molecules and hydroxylated surface, (d–f) shows carvone on a non-hydroxylated surface with 0 water molecules, on a non-hydroxylated surface with 4 water molecules and on a hydroxylated surface. Note a slightly larger TiO_2 system was used for carvone on the non-hydroxylated surface with 4 water molecules to fully accommodate the carvone and water molecules. Red atoms correspond to O atoms, pink atoms correspond to Ti atoms, white atoms correspond to H atoms and cyan atoms correspond to carbon atoms.

surface Ti atoms, allowing the carvone molecule to be in closer proximity to the TiO$_2$ surface.

Interestingly, with the addition of 0.5 ML of water for the non-hydroxylated surface, the free energy of desorption is lowered greatly by $\sim$40 kJ mol^{-1} for limonene, but the free energy of desorption is slightly higher for carvone. In our previous study of the role of hydration on the desorption of limonene from a hydroxylated SiO$_2$ surface, we found the water molecules displace limonene from the surface, thus lowering the desorption energy.[45] While this was the case for limonene in both the non-hydroxylated and hydroxylated surfaces, carvone does not seem to follow this trend for the non-hydroxylated 0.5 ML surface. However, as Table 4 indicates, the carvone molecule does not disrupt the hydrogen bonding network, so the addition of water would not displace carvone

from the surface in the same way as limonene. In addition, we can see this trend by investigating the same disruption of the hydrogen bonding network as a function of distance from the surface, which can be seen in Fig. 5. These results are in agreement with our experimental results that show low amounts of carvone are displaced with the addition of water.

An additional component of our study of the non-hydroxylated 0.5 ML H$_2$O surface is that for both limonene and carvone, the potential of mean force curve shows a kink when the adsorbate is 4 Å from the surface. This occurs when the molecule is removed from the water layer, resulting in a shift in free energy. We do not see this happen in the 1 ML H$_2$O surface system as there are more water molecules so the transition from the water layer to gas phase is less abrupt. The geometries of the adsorbate (where the carvone carbonyl oxygen atom sticks down towards the surface) as they move out of the water layer are discussed in more detail in the ESI.†

Fig. 4(b) shows the desorption free energy for the hydroxylated surfaces which are much lower compared to the free energy of desorption for the non-hydroxylated surface, and this is due to the hydroxylation of surface Ti atoms. When incorporating the role of %RH, limonene, which is easily replaced by water at the surface shows a 20 kJ mol^{-1} decrease in free energy of desorption and carvone shows at 4 kJ mol^{-1} decrease. We attribute this to hydrogen bonds formed between carvone and the surrounding water molecules. Finally, both surfaces
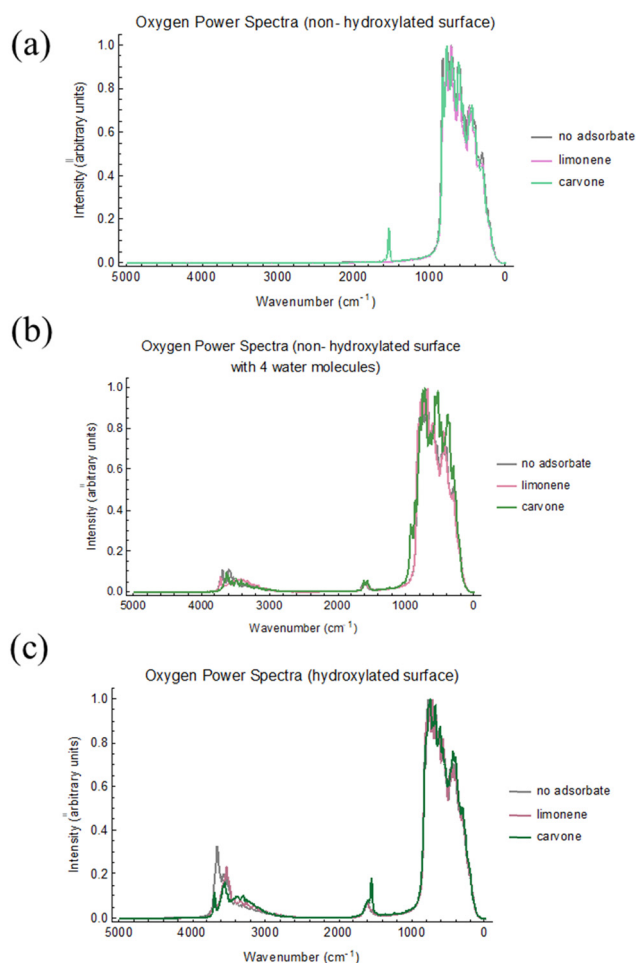

Fig. 7 (a) Oxygen power spectra for the non-hydroxylated TiO$_2$ surface, the non-hydroxylated surface with 1 limonene molecule, and the non-hydroxylated surface with 1 carvone molecule. (b) Oxygen power spectra for the non-hydroxylated TiO$_2$ surface with 4 water molecules, the non-hydroxylated surface with 4 water molecules and 1 limonene molecule, and the non-hydroxylated surface with 4 water molecules and 1 carvone molecule. (c) Oxygen power spectra for hydroxylated surface, hydroxylated surface with limonene molecule, and hydroxylated surface with carvone molecule. All intensity values have been rescaled to run from 0 to 1.
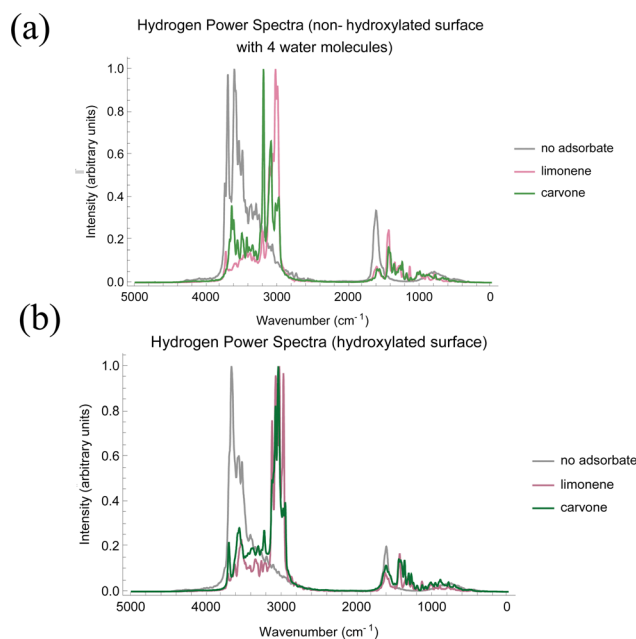

Fig. 8 (a) Hydrogen power spectra for the non-hydroxylated TiO$_2$ surface with 4 water molecules, the non-hydroxylated surface with 4 water molecules and 1 limonene molecule, and the non-hydroxylated surface with 4 water molecules and 1 carvone molecule. (b) Hydrogen power spectra for hydroxylated surface, hydroxylated surface with limonene molecule, and hydroxylated surface with carvone molecule. There are no hydrogen atoms on the non-hydroxylated surface, so no hydrogen power spectrum has been computed. All intensity values have been rescaled to run from 0 to 1.
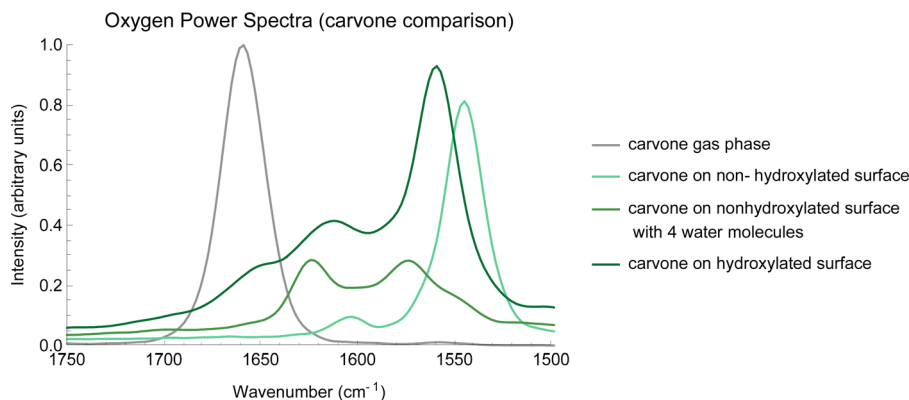
This journal is © the Owner Societies 2022

Phys. Chem. Chem. Phys., 2022, **24**, 23870–23883 | **23879**

Fig. 9 Oxygen power spectra of the carvone carbonyl stretching region. We see red shifting when the carvone molecule is on the surface, and greater red shifting without water/hydroxyl groups. All intensity values have been rescaled to run from 0 to 1 and the spectra for carvone on the TiO$_2$ surfaces has been scaled by 5× for clarity.

show with 1 ML of water, the free energy of desorption is similar for each adsorbate, converging around 28 kJ mol^{-1} for limonene and 50 kJ mol^{-1} for carvone. This further validates our use of two different extrema to describe a real world TiO$_2$ surface.

In order to further investigate the interactions between limonene and carvone on TiO$_2$ surfaces, as well as to provide computational power spectra to compare to our experimental results, *ab initio* Molecular Dynamics simulations (AIMD) of each adsorbate on TiO$_2$ have been performed. Three TiO$_2$ surfaces have been considered to model the TiO$_2$ surface, as detailed in the methods section. First, we have constructed a non-hydroxylated TiO$_2$ surface with surface Ti atoms, secondly, we have constructed a non-hydroxylated TiO$_2$ surface with 4 water molecules, and thirdly, we have constructed a fully hydroxylated surface. Fig. 6 shows each surface with limonene or carvone.

From our simulations, we have constructed the power spectra for the oxygen atoms of each system, as shown in Fig. 7, and the hydrogen atoms of the system, as shown in Fig. 8. Note that the positions and not exact intensities are comparable to experimental data. However, it is reasonable to compare the trends in AIMD power spectra to trends in the experimental FTIR spectra.

Fig. 7 shows consistency between the oxygen power spectra of all three simulated surfaces. For the carvone carbonyl stretch, we see agreement with our experimental results in Fig. S5 (ESI†), where the carbonyl stretch is at a higher wavenumber with the addition of water. In addition, in the hydroxylated surface, Fig. 7c, we see the presence of both the water stretch at 1620 cm^{-1} and the carvone carbonyl stretch at 1575 cm^{-1}. This is more clearly seen in Fig. 9.

According to the hydrogen power spectra, we see a decrease in 3700 cm^{-1} peak with the addition of adsorbate to the surface, which is in agreement with the Ti–OH loss shown in Fig. 2. This results in red shifting of the hydroxyl/water molecules due to the adsorbate on the surface, which is consistent with our classical MD simulations that show the formation of π-hydrogen and hydrogen bonds on the surface. In addition, in

the systems with free water molecules, there was a similar interaction pattern as described in the classical MD simulation section where the adsorbate forms a π-hydrogen or hydrogen bond with a molecule also in a water–water hydrogen bond. Hydrogen bonding statistics for these two surfaces are described in Table 5.

Table 5 shows consistency with our classical MD simulations where limonene can form more π-hydrogen bonds to the surface and surrounding waters compared to carvone, and that carvone can form many hydrogen bonds *via* the oxygen atom to the surface and surrounding waters. In our AIMD simulations, we see there is a higher average number of hydrogen bonds for carvone to the hydroxylated surface compared to the classical MD simulations; however, this difference is consistent with our previous studies of carvone on SiO$_2$. For carvone on the non-hydroxylated TiO$_2$ surface with 4 water molecules, there are fewer hydrogen bonds, and this is due to portions of the trajectory where the carvone oxygen atom is not closely interacting with the surrounding water molecules.

For the non-hydroxylated TiO$_2$ surface with 0 water molecules, we see agreement between the trajectories of our classical MD simulations: the limonene molecule is positioned between two rows of bridging oxygen atoms and the carvone carbonyl oxygen atom is positioned very close to a surface Ti atom, in this case within 2.5 Å during the course of the 30 ps simulation. Using AIMD allows us to better probe the carvone carbonyl

Table 5 Hydrogen bonding statistics for AIMD simulations. The non-hydroxylated surface with 0 water molecules cannot form any hydrogen bonds. Hydrogen bonding criteria was determined if the O–O or O–C$_{sp2}$ distance was less than 3.5 Å and the OH···O angle or OH···C$_{sp2}$ angle was >120°

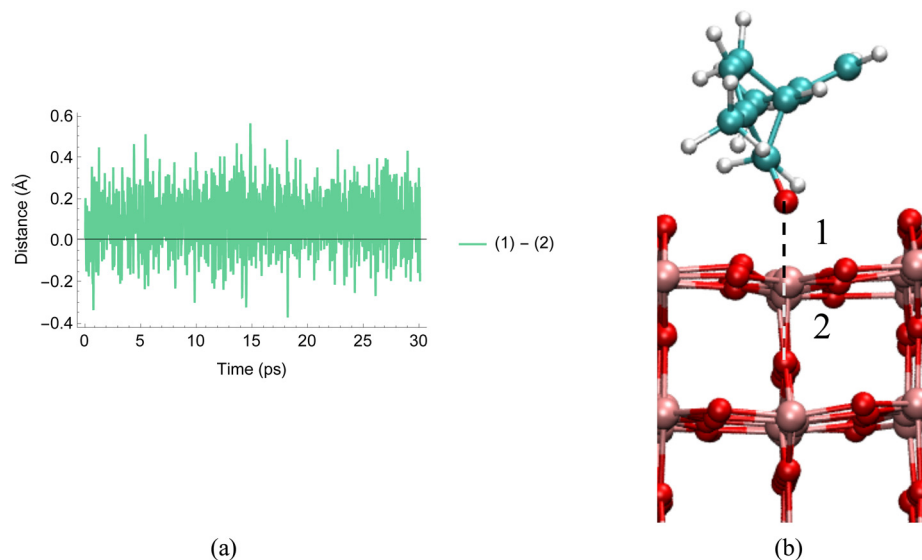| Surface	Average number of π-hydrogen bonds		Average number of hydrogen bonds
	Limonene	Carvone	Carvone
Non-hydroxylated with 4 water molecules	0.18	0	0.98
Hydroxylated	0.35	0.002	1.96

(a)

(b)

Fig. 10 Difference between distance (1) and distance (2) during the course of the 30 ps AIMD simulation.

oxygen–Ti interaction, as Fig. 9 shows the red shift of the carvone carbonyl stretching frequency on the surface.

For the systems with hydrogen atoms, this red shift arises from the carbonyl oxygen forming hydrogen bonds with surrounding hydrogen atoms, at around $\sim 1575\ cm^{-1}$. We see a greater red shift for the non-hydroxylated $0H_2O$ surface, at around $\sim 1525\ cm^{-1}$, which is consistent with our experimental results (Fig. S5, ESI†) that show a peak at $1648\ cm^{-1}$ at $<1\%$ RH and $1660\ cm^{-1}$ with 67% RH.

However, since there are no hydrogen atoms in the non-hydroxylated $0H_2O$ surface, yet we still see a red shift, we can attribute this shift to the interaction between the carvone oxygen atom and surface Ti atom. This is highlighted in Fig. 10, which shows the difference in two key distances during the course of the 30 ps simulation. The first distance is between the carvone oxygen atom and Ti atom (the black dashed in line Fig. 10b) and between the Ti atom and the oxygen atom directly below it (the while dashed line in Fig. 10b). When this difference is negative, it corresponds to the carvone carbonyl oxygen atom being closer to the Ti atom then the crystal oxygen atom. This occurs 20% of the time during the course of the simulation. This result indicates the potential reactivity between oxygenated species and the bare TiO_2 surface and will be addressed in our future work. By looking at the strength of red shifting for the C=O stretch, our AIMD simulations indicate the Ti–O interaction is stronger than the carvone oxygen to water interaction, which is inconsistent with the conclusions of our experimental results. We suggest this is due to the differences between the idealized TiO_2 surfaces used for simulations and the real world TiO_2 surface.

Conclusions

This study investigated the complex interactions of limonene and carvone, indoor relevant organic molecules, with the

hydroxylated TiO_2 surface under different relative humidity conditions using infrared spectroscopy. The IR absorption spectra show that limonene forms $Ti–OH\cdots\pi$-hydrogen bonds with the hydroxylated TiO_2 surface; and our data suggest that carvone initially forms O–H hydrogen bonds (carbonyl $O\cdots HO–Ti$) in addition to the $Ti–OH\cdots\pi$-bonds with the hydroxylated TiO_2 surface, then a stronger bond between carbonyl group and a Ti^{4+} surface atom is formed once all the free Ti–OH function groups on the TiO_2 surface are occupied. An increase in %RH decreases the adsorption of limonene on TiO_2 surface. This is attributed to the completive adsorption of the water coordinated via hydrogen bonding with surface Ti–OH groups. The adsorbed limonene can be completely displaced when the TiO_2 surface is exposed to a relative humidity above 50% RH $(\sim 2$ MLs $H_2O)$. It was found that adsorption strength of carvone on the TiO_2 surface is much stronger than that of limonene, which is supported by the evidence that only 25% of carvone is displaced by the adsorbed water. This implies that the carvone adsorption could significantly inhibit the subsequent interactions of other VOCs, such as limonene, on the TiO_2 surface.

Two kinds of Molecular Dynamics simulations, classical force field-based and *ab initio* molecular dynamics (AIMD) simulations were performed in order to gain an atomistic perspective of the adsorption of limonene and carvone on TiO_2. Due to complications on how to best model the TiO_2 surface, two classical force field-based surfaces and three AIMD surfaces were constructed. These surfaces showed consistency between surface interactions present and provided agreement with the experimental conclusions that the adsorption strength of carvone on the TiO_2 surface is stronger compared to that of limonene. Our results indicate that limonene forms more π-hydrogen bonds with water molecules engaged in hydrogen bonding with the surface, and due to the competitive adsorption of water molecules, suggests why there is a decrease in

This journal is © the Owner Societies 2022

Phys. Chem. Chem. Phys., 2022, **24**, 23870–23883 | **23881**

adsorption of limonene on TiO_2 in surfaces with >1% RH. However, the formation of oxygen hydrogen bonds between carvone and the surrounding water molecules allows carvone to be retained on the TiO_2 surface with increasing relative humidity. In addition, our AIMD simulation of a non-hydroxylated TiO_2 surface suggests an interaction between the carvone oxygen atom and surface Ti atom that may result in surface reactivity. The results further indicate that increases in relative humidity can significantly decrease photocatalytic oxidation efficiency of limonene due to the adsorption of water on the active sites of TiO_2 surface. The role of the adsorbed water in the photocatalytic oxidation of carvone on TiO_2 surface needs further examination. Future studies will focus on the TiO_2 surface chemistry reaction mechanisms of relevant indoor reactive oxygenated species. There are several critical factors such as relative humidity, temperature, and light will be explored.

Author contributions

Hanyu Fan made experimental measurements; Elianna S. Frank performed theoretical simulations. Vicki H. Grassian (oversaw all experimental aspects) and Douglas J. Tobias (oversaw all theoretical aspects) participated in the analysis of results and conclusions and are corresponding authors. All authors contributed to either the writing and/or editing of the manuscript.

Conflicts of interest

The authors declare no competing financial interest.

Acknowledgements

References

1 N. E. Klepeis, W. C. Nelson, W. R. Ott, J. P. Robinson, A. M. Tsang, P. Switzer, J. V. Behar, S. C. Hern and W. H. Engelmann, *J. Exposure Sci. Environ. Epidemiol.*, 2001, **11**, 231–252.

2 J. Wu, Y. Alipouri, H. Luo and L. Zhong, *J. Hazard. Mater.*, 2022, **421**, 126766.

3 E. Gallego, X. Roca, J. F. Perales and X. Guardino, *J. Environ. Sci.*, 2009, **21**, 333–339.

4 V. V. Tran, D. Park and Y.-C. Lee, *Int. J. Environ. Res. Public Health*, 2020, **17**, 2927.

5 I. Rivas, J. Fussell, F. Kelly and X. Querol, *Indoor Air Pollution*, 2019, 1–34, DOI: **10.1039/9781788016179-00001**.

6 C. J. Weschler and N. Carslaw, *Environ. Sci. Technol.*, 2018, **52**, 2419–2428.

7 V. Davamani, D. Mohan, E. Parameswari, S. Arulmani, P. Sebastian and I. Tamilselvan, *Int. Res. J. Pure Appl. Chem.*, 2020, 40–61, DOI: **10.9734/irjpac/2020/v21i930197**.

8 J. P. D. Abbatt and C. Wang, *Environ. Sci.: Processes Impacts*, 2020, **22**, 25–48.

9 EPA, **https://www.epa.gov/indoor-air-quality-iaq/introduction-indoor-air-quality**, in 2021.

10 WHO, **https://www.who.int/news-room/fact-sheets/detail/household-air-pollution-and-health**, in 2021.

11 S. Wang, H. M. Ang and M. O. Tade, *Environ. Int.*, 2007, **33**, 694–705.

12 C. H. Ao and S. C. Lee, *Chem. Eng. Sci.*, 2005, **60**, 103–109.

13 B. Guieysse, C. Hort, V. Platel, R. Munoz, M. Ondarts and S. Revah, *Biotechnol. Adv.*, 2008, **26**, 398–410.

14 P. J. Asilevi, P. Boakye, S. Oduro-Kwarteng, B. Fei-Baffoe and Y. A. Sokama-Neuyam, *Sci. Rep.*, 2021, **11**, 22830.

15 Y. Huang, S. S. Ho, Y. Lu, R. Niu, L. Xu, J. Cao and S. Lee, *Molecules*, 2016, **21**, 56.

16 H. Chen, C. E. Nanayakkara and V. H. Grassian, *Chem. Rev.*, 2012, **112**, 5919–5948.

17 D. B. Collins and D. K. Farmer, *Environ. Sci. Technol.*, 2021, **55**, 12172–12179.

18 Z. Shayegan, C.-S. Lee and F. Haghighat, *Chem. Eng. J.*, 2018, **334**, 2408–2439.

19 H. Yu, K. Zhang and C. Rossi, *Indoor Built Environ.*, 2007, **16**, 529–537.

20 A. Rabajczyk, M. Zielecka, W. Klapsa and A. Dziechciarz, *Materials*, 2021, **14**, 2161.

21 M. Pelaez, N. T. Nolan, S. C. Pillai, M. K. Seery, P. Falaras, A. G. Kontos, P. S. M. Dunlop, J. W. J. Hamilton, J. A. Byrne, K. O'Shea, M. H. Entezari and D. D. Dionysiou, *Appl. Catal., B*, 2012, **125**, 331–349.

22 A.-I. Gopalan, J.-C. Lee, G. Saianand, K.-P. Lee, P. Sonar, R. Dharmarajan, Y.-L. Hou, K.-Y. Ann, V. Kannan and W.-J. Kim, *Nanomaterials*, 2020, **10**, 1854.

23 L. Frazer, *Environ. Health Perspect.*, 2001, **109**, A174–A177.

24 F. Thevenet, L. Olivier, F. Batault, L. Sivachandiran and N. Locoge, *Chem. Eng. J.*, 2015, **281**, 126–133.

25 H. O. Seo, D. Kim, K.-D. Kim, E. J. Park, C. Sim and Y. D. Kim, *Adsorption*, 2013, **19**, 1181–1187.

26 A. H. Mamaghani, F. Haghighat and C.-S. Lee, *Appl. Catal., B*, 2017, **203**, 247–269.

27 A. P. Ault, V. H. Grassian, N. Carslaw, D. B. Collins, H. Destaillats, D. J. Donaldson, D. K. Farmer, J. L. Jimenez, V. F. McNeill, G. C. Morrison, R. E. O'Brien, M. Shiraiwa, M. E. Vance, J. R. Wells and W. Xiong, *Chem*, 2020, **6**, 3203–3218.

28 Y. Liu, A. G. Bé, V. W. Or, M. R. Alves, V. H. Grassian and F. M. Geiger, *Cell Rep. Phys. Sci.*, 2020, **1**, 100256.

29 A. H. Mamaghani, F. Haghighat and C.-S. Lee, *Build. Environ.*, 2021, **189**, 107518.

30 F. Batault, F. Thevenet, V. Hequet, C. Rillard, L. Le Coq and N. Locoge, *Chem. Eng. J.*, 2015, **264**, 197–210.

31 M. Nagao and Y. Suda, *Langmuir*, 1989, **5**, 42–47.

32 M. Singh, N. Zhou, D. K. Paul and K. J. Klabunde, *J. Catal.*, 2008, **260**, 371–379.

33 M. R. Alves, Y. Fang, K. J. Wall, V. Vaida and V. H. Grassian, *J. Phys. Chem. A*, 2019, **123**, 7661–7671.

34 M. R. Nimlos, E. J. Wolfrum, M. L. Brewer, J. A. Fennell and G. Bintner, *Environ. Sci. Technol.*, 1996, **30**, 3102–3110.

23882 | *Phys. Chem. Chem. Phys.*, 2022, **24**, 23870–23883

This journal is © the Owner Societies 2022

35 T. N. Obee and R. T. Brown, *Environ. Sci. Technol.*, 1995, **29**, 1223–1231.

36 R. M. Alberici and W. F. Jardim, *Appl. Catal., B*, 1997, **14**, 55–68.

37 L. Zhong, C.-S. Lee and F. Haghighat, *J. Hazard. Mater.*, 2012, **243**, 340–349.

38 L. Huang, E. S. Frank, M. Shrestha, S. Riahi, D. J. Tobias and V. H. Grassian, *Environ. Sci. Technol.*, 2021, **55**, 6623–6630.

39 A. K. Boulamanti and C. J. Philippopoulos, *Atmos. Environ.*, 2009, **43**, 3168–3174.

40 A. K. Boulamanti, C. A. Korologos and C. J. Philippopoulos, *Atmos. Environ.*, 2008, **42**, 7844–7850.

41 G. Rubasinghege and V. H. Grassian, *Chem. Commun.*, 2013, **49**, 3071–3094.

42 D. Vildozo, R. Portela, C. Ferronato and J.-M. Chovelon, *Appl. Catal., B*, 2011, **107**, 347–354.

43 L. Zhang, W. Anderson, S. Sawell and C. Moralejo, *Chemosphere*, 2007, **68**, 546–553.

44 Q. Geng, Q. Guo and X. Yue, *Ind. Eng. Chem. Res.*, 2010, **49**, 4644–4652.

45 E. S. Frank, H. Fan, M. Shrestha, S. Riahi, D. J. Tobias and V. H. Grassian, *J. Phys. Chem. A*, 2020, **124**, 10592–10599.

46 Y. Fang, P. S. J. Lakey, S. Riahi, A. T. McDonald, M. Shrestha, D. J. Tobias, M. Shiraiwa and V. H. Grassian, *Chem. Sci.*, 2019, **10**, 2906–2914.

47 H. Fan, E. S. Frank, P. S. J. Lakey, M. Shiraiwa, D. J. Tobias and V. H. Grassian, *J. Phys. Chem. C*, 2022, **126**, 6267–6279.

48 G. Munuera and F. S. Stone, *Discuss. Faraday Soc.*, 1971, **52**, 205–214.

49 C. Zhang and P. J. D. Lindan, *J. Chem. Phys.*, 2004, **121**, 3811–3815.

50 P. J. D. Lindan, N. M. Harrison and M. J. Gillan, *Phys. Rev. Lett.*, 1998, **80**, 762–765.

51 L. A. Harris and A. A. Quong, *Phys. Rev. Lett.*, 2004, **93**, 086105.

52 L.-M. Liu, C. Zhang, G. Thornton and A. Michaelides, *Phys. Rev. B: Condens. Matter Mater. Phys.*, 2010, **82**, 161415.

53 J. Margineda and N. J. English, *Chem. Phys. Lett.*, 2020, **743**, 137164.

54 Materials Project. **https://Materialsproject.Org/Materials/Mp-2657/**.

55 E. G. Brandt and A. P. Lyubartsev, *J. Phys. Chem. C*, 2015, **119**, 18110–18125.

56 W. L. Jorgensen, J. Chandrasekhar, J. D. Madura, R. W. Impey and M. L. Klein, *J. Chem. Phys.*, 1983, **79**, 926–935.

57 LAMMPS Molecular Dynamics Simulator. **https://lammps.sandia.gov/index.html** (accessed Feb 25, 2020).

58 H. C. Andersen, *J. Comput. Phys.*, 1983, **52**, 24–34.

59 R. E. Isele-Holder, W. Mitchell and A. E. Ismail, *J. Chem. Phys.*, 2012, **137**, 174107.

60 D. J. Evans and B. L. Holian, *J. Chem. Phys.*, 1985, **83**, 4069–4074.

61 G. M. Torrie and J. P. Valleau, *J. Comput. Phys.*, 1977, **23**, 187–199.

62 A. Grossfield, "WHAM: the weighted histogram method", version 2.0.9.1. **https://membrane.urmc.rochester.edu/?page_id=126** (accessed Mar 11, 2020).

63 J. P. Perdew, K. Burke and M. Ernzerhof, *Phys. Rev. Lett.*, 1996, **77**, 3865–3868.

64 J. VandeVondele and J. Hutter, *J. Chem. Phys.*, 2007, **127**, 114105.

65 S. Grimme, J. Antony, S. Ehrlich and H. Krieg, *J. Chem. Phys.*, 2010, **132**, 154104.

66 T. D. Kühne, M. Iannuzzi, M. D. Ben, V. V. Rybkin, P. Seewald, F. Stein, T. Laino, R. Z. Khaliullin, O. Schütt, F. Schiffmann, D. Golze, J. Wilhelm, S. Chulkov, M. H. Bani-Hashemian, V. Weber, U. Borštnik, M. Taillefumier, A. S. Jakobovits, A. Lazzaro, H. Pabst, T. Müller, R. Schade, M. Guidon, S. Andermatt, N. Holmberg, G. K. Schenter, A. Hehn, A. Bussy, F. Belleflamme, G. Tabacchi, A. Glöß, M. Lass, I. Bethune, C. J. Mundy, C. Plessl, M. Watkins, J. VandeVondele, M. Krack and J. Hutter, *J. Chem. Phys.*, 2020, **152**, 194103.

67 J. VandeVondele and J. Hutter, *J. Chem. Phys.*, 2003, **118**, 4365–4369.

68 P. Pulay, *J. Comput. Chem.*, 1982, **3**, 556–560.

69 M. Thomas, M. Brehm, R. Fligg, P. Vöhringer and B. Kirchner, *Phys. Chem. Chem. Phys.*, 2013, **15**, 6608–6622.

70 M. Brehm and B. Kirchner, *J. Chem. Inf. Model.*, 2011, **51**, 2007–2023.

71 A. L. Goodman, E. T. Bernard and V. H. Grassian, *J. Phys. Chem. A*, 2001, **105**, 6443–6457.

This journal is © the Owner Societies 2022

Phys. Chem. Chem. Phys., 2022, **24**, 23870–23883 | 23883